ORIGINAL ARTICLE

Large Piezoelectric Response and Ferroelectricity in Li and V/Nb/Ta co-doped *w*-AlN

Mohammad Noor-A-Alam[1], **Oskar Z. Olszewski**[1] , **Humberto Campanella**[1] **and Michael Nolan**[1,2]

1. Tyndall National Institute, Lee Maltings, Dyke Parade, University College Cork, Cork, T12 R5CP, Ireland

2. NIBEC, School of Engineering, Ulster University, Shore Road, Antrim, Northern Ireland

Correspondence
Email: mda.alam@tyndall.ie, michael.nolan@tyndall.ie

Funding information
Science Foundation Ireland (SFI), European Regional Development Fund

Based on density functional theory, we show that Li and X (X=V, Nb and Ta) co-doping in 1Li:1X ratio broadens the compositional freedom for significant piezoelectric enhancement in *w*-AlN, promising them to be good alternatives of expensive Sc. Interestingly, these co-doped *w*-AlN also show quite large spontaneous electric polarization about 0.80 C/m^2 with the possibility of ferroelectric polarization switching, opening new possibilities in wurtzite nitrides. Increase in piezoelectric stress constant (e_{33}) with decrease in elastic constant (C_{33}) results enhancement in piezoelectric strain constant (d_{33}), which is desired for improving the performance of resonators for high frequency RF signals. Also, these co-doped w-AlN are potential lead-free piezoelectric materials for energy harvesting and sensors as they improve the longitudinal electromechanical coupling constant (K_{33}^2), transverse piezoelectric strain constant (d_{31}), and figure of merit for power generation. However, the enhancement in K_{33}^2 is not as pronounced as that in d_{33} , because co-doping increases dielectric constant. The longitudinal acoustic wave velocity (7.09 km/s) of $Li_{0.1875}Ta_{0.1875}Al_{0.625}N$ is quite comparable with that of commercially used piezoelectric $LiNbO_3$

or $LiTaO_3$ in special cuts (about 5~7 km/s) despite the fact that the acoustic wave velocities drop with co-doping or Sc concentration.

Keywords: DFT, Piezoelectricity, Ferroelectricity, *w*-AlN, Nitrides, Doping.

1 | INTRODUCTION

Aluminum Nitride in the wurtzite crystal structure (*w*-AlN) is an excellent piezoelectric material for resonators such as thin-film bulk acoustic resonators (FBARs) and solidly mounted resonators (SMRs), which are promising for radio frequency (RF) filters for telecommunication systems that operate at over 5 GHz[1, 2, 3, 4, 5, 6]. The key advantages of *w*-AlN are its high Curie temperature of 1150°C, high acoustic velocity, high quality (*Q*) factor, low acoustic losses, chemical stability and more importantly its compatibility with CMOS technology, which allow foundry process line and tool sharing, and open the way for system-on-chip integration[1, 2, 3, 4, 5, 7, 8, 9]. However, its rather low electromechanical coupling limits the bandwidth, which is one of the main challenges for its applications in wide band communication systems[1, 2, 3, 4, 5, 6].

Recently large enhancement in piezo-response (d_{33}) and electromechanical coupling (K_{33}^2) has been discovered in Sc doped *w*-AlN[10, 11, 12]. Interestingly, ferroelectricity with large electric polarization (~ 1 C/m^2) has been predicted[13] and recently demonstrated for Sc doping, although the coercive field in the range of few MV/cm [14], and the atomistic origin of this large coercive field is unclear. However, search for suitable dopants to replace Sc is of great scientific as well as industrial importance as Sc is an expensive and scarce element. In general, ions with high charge states (e.g., 4+ or 5+) can enhance ionic contribution to the piezoelectric stress constant e_{33}, hence might improve d_{33}. In this regard, based on density functional theory (DFT), a set of divalent cation (e.g., Mg^{2+}, Ca^{2+} and Zn^{2+}) and tetravalent cation (e.g., Hf^{4+}, Zr^{4+}, and Ti^{4+}) has been predicted for significant enhancement of piezo-response in *w*-AlN[15, 16]. The ratio of divalent and tetravalent cations is kept 1:1 for the charge neutrality. In other words, two Al atoms are replaced by 1 divalent atom and 1 tetravalent atom. Recently, $(Mg,Hf)_xAl_{1-x}N$ films ($0 < x < 0.24$) with a composition-gradient has been grown on a Si(100) substrate at 600°C by co-sputtering from AlN and MgHf targets[17]. This high-throughput/combinatorial approach for Mg and Hf co-doping has demonstrated a promisingly large piezo-response and power generation figure of merit suitable for energy harvesting[17]. Enhancement of piezoelectricity in several other quaternary alloys based on divalent and tetravalent cations in *w*-AlN (e.g., (Mg,Ti)AlN[18, 19], (Mg,Zr)AlN[20, 21], and (Zn,Ti)AlN[19]) has also been confirmed experimentally. Moreover, a giant increase of d_{33} in w-AlN by co-doping of divalent Mg and pentavalent Nb has been predicted by the first principles calculations[22] and also later confirmed experimentally[23]. The optimized atomic ratio between $Nb^{5+}$and Mg^{2+} ions in *w*-AlN is 1:2 for obtaining the best piezoelectric response[23] because this ratio ensures the charge neutrality. Furthermore, the co-doping of divalent and tetravalent/pentavalent in these cases are essential as the single dopants e.g., Mg[23, 19], Zn[19], Ti[19], and Nb[23] in *w*-AlN not only have negative impact on the crystalline quality but also are ineffective for piezoelectricity enhancement. Note that aforementioned dopants in *w*-AlN are metastable and inaccessible through thermodynamic equilibrium synthesis process because of phase separation (e.g. rocksalt ScN and wurtzite AlN)[11, 17, 18, 13]. However, reactive magnetron sputtering, which is a physical vapor deposition (PVD) technique allows such metastable doping that broadens the compositional freedom for dopants, opening a large possibility of designing new multi-functional materials[11, 17, 18, 13, 24].

Evidently, a general trend is choosing elements that show large ionic radius – preferably close to that of Sc^{3+}

(88.5 pm) – and large charge state (e.g., 4+ or 5+) for enhancing piezo-response in *w*-AlN. This inspires us to study simultaneous doping of monovalent Li (ionic radius of 90pm) and pentavalent V/Nb/Ta (ionic radius of 68/78/78 pm, respectively) in 1:1 atomic ratio. Our first principles calculations show that this co-doping significantly improves the piezoelectric response of *w*-AlN. Our finding broadens compositional freedom to enhance the d_{33} in *w*-AlN, hence potential replacement of expensive Sc doping. Moreover, these co-doping introduces possibility of ferroelectricity in non-ferroelectric *w*-AlN. We estimate the coercive field (E_c) qualitatively, and find that the large E_c (in the range of few MV/cm) is due to the large energy difference between ferroelectric wurtzite and paraelectric hexagonal phase. Interestingly, the spontaneous electric polarization decreases as a function of co-doping concentration, although a quite large polarization (~0.80 C/m^2) still remains at 37.5% co-doping, which is comparable to that of pervoskites e.g $PbTiO_3$. Additionally, we investigate various properties – namely elastic properties, electromechanical coupling, dielectric constant, and acoustic velocities – that are important parameters for designing piezoelectric devices such resonators, sensors, and energy harvesters. Promisingly, these properties are also quite comparable with these of Sc doped *w*-AlN.

2 | COMPUTATIONAL DETAILS

Our first-principles calculations are performed in the framework of spin-polarized density functional theory using projector augmented wave (PAW) potentials to describe the core electrons and the generalized gradient approximation (GGA) of Perdew, Burke, and Ernzernhof (PBE) for exchange and correlation as implemented in the Vienna Ab initio Simulation Package (VASP) [25, 26, 27] based on a plane-wave basis set. The number of valence electrons for Al, N, Li, V, Nb, and Ta are 3, 5, 1, 11, 11, and 11, respectively. On-site U corrections (GGA+U) for *d* state of V, Nb and Ta are 3eV, 2.95eV and 2.95eV, respectively[28, 29, 30]. There is no magnetic moment observed, which is expected for pentavalent V, Nb and Ta ions. A cutoff energy of 500 eV for the plane-wave expansion is used in all calculations. All the structures are fully relaxed until the Hellmann-Feynman forces on each atom are less than 10^{-3} eV/Å. The lattice parameters and internal coordinates of the structures are fully relaxed to achieve the lowest energy configurations. Geometry optimization is carried out employing the conjugated gradient technique and the convergence for the total energy is set as 10^{-6} eV. The wurtzite supercells with 32 atoms are generated using the special quasirandom structures (SQS)[31]. For Li and X co-doped supercells, first we generate an SQS configuration at a particular concentration, then another configuration is generated by just interchanging the atomic positions of Li and X. For Sc doping, we consider an SQS supercell and a manually created supercell. The structural information of the relaxed supercells are given in the "Supplementary Information". For both Sc and co-doping, all the results reported in this paper are average over the values obtained from the two considered supercells at a particular concentration. The Brillouin zone is sampled with a Γ-centered *k*-point mesh of $6 \times 6 \times 6$ for all the calculations. Density functional perturbation theory (DFPT) is used to calculate elastic C_{ij}, Born effective charges (Z^*_{ij}) and piezoelectric e_{ij} tensors. Using DFPT, we also qualitatively estimate the macroscopic dielectric constant (high frequency dielectric constant including local field effects or electronic contribution $\varepsilon^{\infty}_{33}$ plus the static dielectric constant or ionic contribution ε^{0}_{33}).

3 | RESULTS AND DISCUSSION

First, we examine how the doping changes the ratio of the lattice parameters *a* and *c* (i.e., *c/a* ratio) in *w*-AlN, which plays an important role in the origin of electric polarization as well as the piezoelectric response of wurtzites[32, 33]. Usually wurtzite crystals with smaller *c/a* ratio show higher piezoelectric response[32]. Our calculated *c/a* ratio of

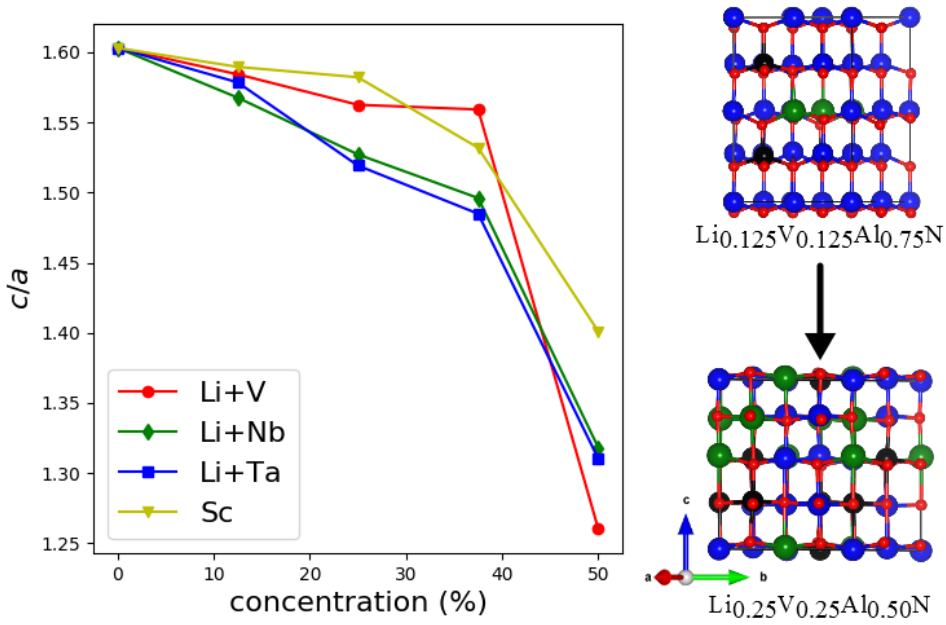

FIGURE 1 The change in *c/a* ratio as a function of doping concentration in *w*-AlN. The atomic structures of 25% and 50% Li and V co-doped *w*-AlN. The blue, red, green, and black balls represent Al, N, Li, and V atoms, respectively. The atomic planes of cations and anions for 50% co-doping are almost flat, and the structure resembles hexagonal BN structure. This also reflects in its low *c/a* ratio.

w-AlN (1.603) is comparable with the value of 1.587 obtained experimentally[34]. The *c/a* ratio of *w*-AlN decreases as the doping concentration increases for both co-doping and Sc doping (see Figure 1). Both experiments and first principles calculations have already confirmed this decrease of the *c/a* ratio for Sc doping[34, 35] as well as other dopants[23, 36, 15]. We notice a sharp drop in *c/a* ratio for all the co-doping above concentration of 37.5% (see Figure 1), indicating a phase transition from wurtzite to hexagonal (*h*-BN like structure) phase. For example, the *c/a* ratio of 50% Li and V co-doped structure is almost equal to that of *h*-AlN (1.24) (see Figure 1). Pictorially, we also see that the anions and cations in the optimized 50% Li and V co-doped structure are in almost same atomic-plane (i.e., flat plane), whereas they show wurtzite-like buckled atomic-layers for 25% co-doping (see Figure 1). Such structural change is also observed for Mg and Nb co-doping in *w*-AlN[23]. Note that *h*-AlN exhibits neither spontaneous electric polarization nor piezoelectricity, although the doped *h*-AlN structures may show piezoelectric response because the doping lowers the symmetry locally. In this paper, we limit the doping concentration maximum of 37.5% as we mainly focus on the ferroelectricity and piezoelectricity.

We investigate the elastic properties of the single crystalline co-doped and Sc doped *w*-AlN. First, we check the mechanical stability under the co-doping. Elastic stiffness coefficients for a mechanically stable crystal satisfy Born stability criteria as the elastic energy must be positive. The elastic constants of the co-doped or Sc doped *w*-AlN should satisfy the stability criteria: $C_{11} > 0, (C_{11} - C_{12}) > 0, C_{44} > 0, (C_{11} + C_{12})C_{33} > 2C_{13}^2$[37]. All our co-doped $Li_{x/2}X_{x/2}Al_{1-x}N$ and Sc doped $Sc_xAl_{1-x}N$ (x=0-0.375) structures satisfy the stability criteria (C_{11}, C_{12}, and C_{44} are provided in "Supplementary Information"). The Figure 2(a) shows that all the co-dopants satisfy the $(C_{11} + C_{12})C_{33} > 2C_{13}^2$ criterion. However, generally it is difficult to grow single crystal, hence the single crystal elastic constants are not measured in experiments – rather usually some bulk elastic properties such as Young's moduli (Y), bulk moduli (B), shear moduli (G) and Poisson ratio (υ) are measured. We use Voigt- Reuss-Hill scheme[38] based on the single crystal stiffness constants for calculating Y, B, G and υ. For polycrystalline materials, the Voigt's (V) and the Reuss's (R) approximations provide the upper and lower bounds to the modulus, respectively. The Hill's average (H) is their arithmetic middle value, which is used in this work for the elastic properties of polycrystalline $Li_{x/2}X_{x/2}Al_{1-x}N$ and $Sc_xAl_{1-x}N$ (x=0-0.375) obtained from the ELATE code[38], shown in the Figure 2. All the co-dopants and Sc reduce the polycrystalline Young's modulus (Y), which is expected because the C_{33} decreases with increase in co-doping or Sc concentration. Our calculated Y for Sc doping is comparable with that of the experimentally reported values[39]. Generally, the B/G ratio can be considered as a criterion for ductility or brittleness. The lower/higher the B/G ratio is, the more brittle/ductile the material is. The critical value for B/G is about 1.75, which separates ductile and brittle materials. Poisson ratio (υ) is another indicator of ductility or brittleness. Generally, materials with Poisson ratio lower (higher) than 0.26 are brittle (ductile). Interestingly, we find that both co-doping and Sc doping above 25% transforms brittle *w*-AlN to ductile (Figure 2(c,d)). In fact, Figure 2(b,c) shows that 37.5% Sc doping makes the *w*-AlN remarkably softer compared to the co-dopants.

We calculate total d_{33} and effective $d_{33,f}$ considering the relations $d_{ij} = \sum_{k=1}^{6} e_{ik}(C^{-1})_{kj}$ and $d_{33,f} = e_{33}/C_{33}$, receptively, where d_{ij}, e_{ij} and C_{ij} are piezoelectric strain, piezoelectric stress and elastic tensors, respectively. In the definition of $d_{33,f}$, contributions from in-plane components of e_{ij} and C_{ij} tensors are ignored. It is assumed that the piezoelectric thin films can mainly change geometry along out-of-plane as the in-plane geometry change of the thin films is prevented by the rigidity of the substrate lattice[40]. The d_{33} and the $d_{33,f}$ of *w*-AlN are 4.08 pC/N and 5.27 pC/N, respectively, which are in good agreement with the experimentally reported values of 4.0 pC/N and 5.56 pC/N, respectively[40]. All the co-dopants increase both the total d_{33} and the $d_{33,f}$ of *w*-AlN (shown in Figure 3(a), (b)). For comparison, we calculate the d_{33} and the $d_{33,f}$ as function of Sc concentration in *w*-$Sc_xAl_{1-x}N$ (x=0-0.375), which are quite comparable with previously reported experimental[10, 11] and theoretical values[41, 12, 35]. Additionally, Figure 3(a) shows a good agreement between our measured and calculated d_{33} for *w*-AlN as well as Sc doping. The samples were grown by RF-sputtering, and the d_{33} is measured using a piezometer. We find that our highest total d_{33} for

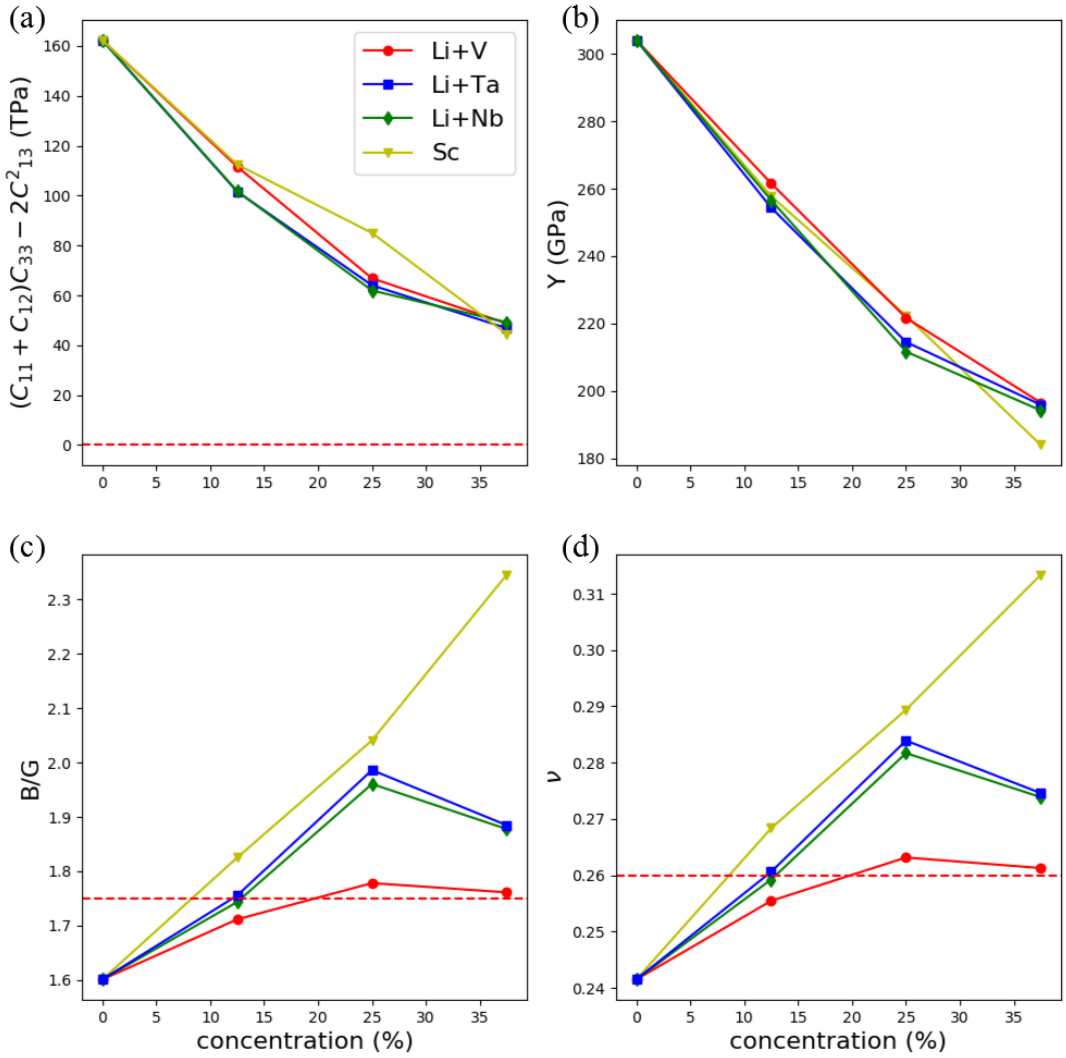

FIGURE 2 The Hill's average of (a) Youngus modulus (Y), (b) Bulk modulus to shear modulus ratio (B/G), and (c) Poission's ratio (υ) as a function of Sc and co-doping concentration in w-AlN. The Hill's average is emplyed for considering the pollycrystallinity of the real doped materials. The red doted line represents the critical value of B/G or υ that separate ductile from brittle behaviour of a material.

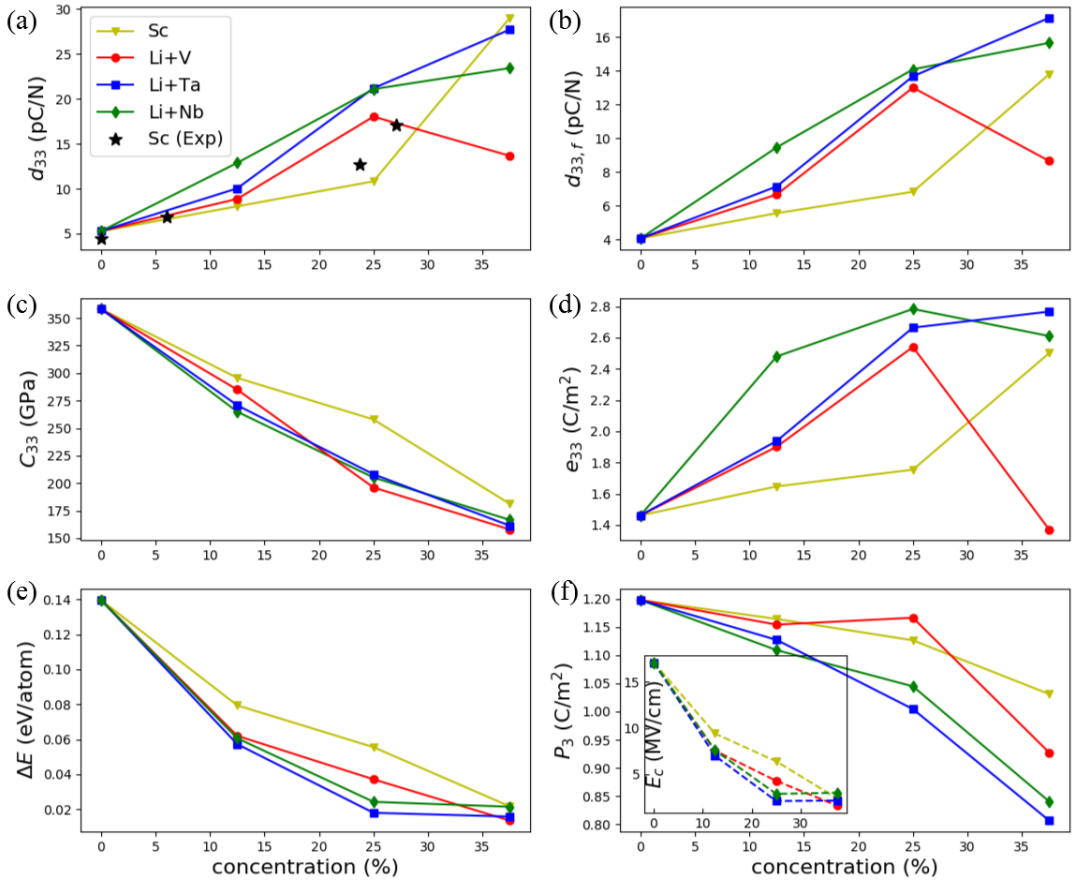

FIGURE 3 (a) The calculated piezoelectric strain constant d_{33} from the relation $d_{ij} = \sum_{k=1}^{6} e_{ik}(C^{-1})_{kj}$, where all the components of piezoelectric stress constants (e_{ij}) and elastic constants (C_{ij}) contribute to d_{ij}, (b) the effective $d_{33,f} = e_{33}/C_{33}$, where it is assumed that the piezoelectric film is only operating along c-axis and the film is clamped to the substrate, (c) the elastic constant C_{33}, (d) the piezoelectric stress constants e_{33}, (e) the energy difference ($\triangle E$) between the wurtzite and hexagonal (crystal structure of hexagonal Boron Nitride) phase of co-doped and Sc doped AlN, which is the estimated energy barrier for polarization switching and (f) the spontaneous electric polarization P_3 as a function of co-doping and Sc doping concentration in w-AlN. Experimental d_{33} for Sc doping in (a) are our own. The coercive field (E_c) as a function of concentration is shown in the inset of (f).

$Li_{0.1875}Ta_{0.1875}Al_{0.625}N$ is slightly lower than that of $Sc_{0.375}Al_{0.625}N$ (see Figure 3(a)). However, $d_{33,f}$ of $Sc_{0.375}Al_{0.625}N$ is about 3.34 pC/N lower than that of $Li_{0.1875}Ta_{0.1875}Al_{0.625}N$ (see Figure 3(b)), indicating that contributions from in-plane components of e_{ij} and C_{ij} tensors to d_{33} are larger in $Sc_{0.375}Al_{0.625}N$ compared to the co-dopants. In fact, d_{33} and $d_{33,f}$ of 12.5% Li and V/Nb/Ta co-doped *w*-AlN are also slightly larger than that of 12.5% Sc doped *w*-AlN (shown in Figure 3(b)). For example, compared to pure *w*-AlN ($d_{33,f}$ = 4.08 pC/N), 12.5% Li+Nb co-doping ($d_{33,f}$ = 9.47 pC/N) enhance $d_{33,f}$ about 132.1%, whereas Sc doping ($d_{33,f}$ = 5.57 pC/N) enhances $d_{33,f}$ by 36.5%. Promisingly, all the co-dopants at 25% show significantly larger d_{33} and $d_{33,f}$ compared to these of 25% Sc doped *w*-AlN (see Figure 3(a-b)). Therefore, Li+V/Nb/Ta co-doping can be good alternatives of Sc doping in terms of piezoelectric response. Also, d_{33} and $d_{33,f}$ of these co-dopants in the doping range of 0-37.5% are quite comparable with these of other reported co-dopants e.g., 1pentavalent:1bivalent[23, 36] or 1tetravalent:1bivalent[15, 16] co-doping.

The enhancement in d_{33} and $d_{33,f}$ is mainly due to the softening of elastic constant C_{33} and increase of e_{33} as the concentration of co-dopants increases (shown in Figure 3(c,d)). Similar mechanism is observed in other dopants e.g., Sc[35] or other dopants[15, 36, 22]. Figure 1 indicates that these dopants lead the polar wurtzite structure close to a phase transition to non-polar hexagonal structure, which results in the softening of C_{33}[35, 12]. In fact, the energy difference between wurtzite and hexagonal phase ($\Delta E = E_{\mathrm{hexagonal}} - E_{\mathrm{wurtzite}}$) becomes significantly smaller with the co-doping or Sc concentration – shown in Figure 3(e). This also indicates the energy proximity of the phase transition[35]. Moreover, the ΔE can be considered as the energy barrier for ferroelectric polarization switching, where non-polar hexagonal phase acts as a paraelectric for a polarization switching from up to down. Obviously, the switching is assumed to occur by a uniform polarization change through a nonpolar high symmetry state, where formation of domains, effect of vacancies, effect of surface charges (depolarization field) in ultrathin films, and effect of electrodes are ignored for computational simplicity. Similar approach was also employed to predict ferroelectricity as well as to estimate ferroelectric switching barrier for hyperferroelectrics[42] and Sc doped *w*-AlN[13], which has been confirmed experimentally later[14]. Interestingly, switching energy barrier is tunable by doping concentration as it decreases with concentration (shown in Figure 3(e)). Also, our calculated energy barriers are comparable to these of Sc doped *w*-AlN[13].

We calculate the spontaneous polarization by $P_3 = \frac{e}{V}\sum_k Z^*_{k,33}\Delta u_{k,3}$, where $Z^*_{k,33}$is the 33 (3 represents crystal's c-direction) component of Born effective charge tensor of *k*-th atom in the supercell, $\Delta u_{k,3}$ is the atomic displacement along the c-direction of *k*-th atom with respect to the ideal nonpolar hexagonal configuration, *e* is the magnitude of an electron's charge and *V* is the polar supercell's volume[14, 43]. The calculated polarization as a function of co-doping and Sc doping concentration is shown in Figure 3(f). The polarization decreases with co-doping or Sc doping concentration, which is expected as the doping lowers the *c*/*a* ratio (see Figure 1) and leads the polar structures closer to the non-polar hexagonal structures. However, our obtained polarization values are quite comparable to that of pervoskites e.g., $PbTiO_3$[44]. Now, to qualitatively estimate the coercive field (E_c) from the energy barrier for the ferroelectric switching (ΔE), we express $E_c(t,T) = \frac{\triangle E - K_B T ln(\frac{\vartheta_0 t}{ln2})}{V^* P_3}$, where t, T, K_B, ϑ_0, $V^*$and P_3 represent the measurement time (t is set to 60s following the Ref[14]), temperature (300K), Boltzmann constant, the attempt frequency ($10^{12}\mathrm{Hz}$, which is a typical optical phonon frequency), the volume of the elementary nucleation site (we consider the supercell as a nucleation site), and the spontaneous polarization, respectively[45]. The estimated E_c are shown in the inset of Figure 3(f). Our estimated E_c (2.35 MV/cm) for 37.5% Sc doped *w*-AlN is quite comparable with that of experimentally measured value of about 2.5 MV/cm for 36% Sc doping[13]. We notice that the E_c decreases – expected as the ΔE decreases – when the Sc or the co-doping concentration increases (See Figure 3(e) and inset of 3(f)), which is also experimentally observed for Sc doping[14]. Interestingly, the E_c for 25% co-doping is much lower than that of 25% Sc doping, rather as low as that of 37.5% Sc doping, indicating the possibility of observing ferroelectric hysteresis loop using reasonable electric field below about 2.5 MV/cm as beyond 4 MV/cm could not be physically realizable without damaging the samples adversely.

However, a thorough investigation, beyond the scope of this paper, on the domain formations, the thickness dependence, and the surface effects will be needed for a deeper understanding. Note that the high E_c in the range of 0.8-2 MV/cm is reported for doped HfO_2, where the large E_c is found beneficial for ferroelectric field-effect-transistors (FeFETs)[46, 47]. In ferroelectric HfO_2, the low dielectric constant typically about 30 and the large E_c promotes ferroelectricity in the thickness range of 5–30 nm, which is usually very challenging for ferroelectric perovskites[46, 47]. Interestingly, we find that Sc doped as well as the co-doped *w*-AlN also show as low dielectric constant (see Figure 5(b)) as that of ferroelectric HfO_2. Therefore, these doped *w*-AlN can be promising ferroelectrics at nanoscale.

To understand the origin of the e_{33} enhancement, we express e_{33} (e_{33}=e_{33}^{ele}+e_{33}^{int}) in terms of (i) the electronic contribution (e_{33}^{ele}) and (ii) the contribution from the internal coordinates of atoms (e_{33}^{int}) in response to an external strain along *c*-direction (η_3)[43, 48, 16]. We find that the large increase of e_{33} is the result of simultaneous significant increase in e_{33}^{int} but decrease in the magnitude of e_{33}^{ele} as a function of co-doping concentration (see Figure 4(a-b)). In contrast, the $|e_{33}^{ele}|$ of Sc doping slightly increases with concentration (see Figure 4(b)) – in agreement with the previous calculations[35]. In fact, the e_{33}^{int} ($|e_{33}^{ele}|$) for all the co-dopants at 25% concentration is quite significantly larger (smaller) than that of the Sc doped *w*-AlN, which guarantees the larger e_{33} (Fig.3(d)) for the co-doping compared to that of 25% Sc doping. From Fig.4(a-b), we see that the sudden big drop in e_{33} for 37.5% Li and V co-doping is solely due to the significant decrease of the e_{33}^{int} as the e_{33}^{ele} remains almost unchanged. For further insights, note that the e_{33}^{int} is proportional to the Born effective charge (Z_{33}) of the ions and the sensitivity ($\frac{du_3}{d\eta_3}$) of the atomic positions (u_3) in response to the strain along *c*-direction (η_3). For the wurtzite structure, the e_{33}^{int} equals to $\sum_i \frac{2e}{\sqrt{3}a_s^2} Z_{33}(i) \frac{du_3(i)}{d\eta_3}$, where *i* runs over all the atoms in the supercell, a_s is the in-plane lattice parameter of the supercell, and *e* is the electron charge[43, 48, 16]. It is convenient to consider an average value of Z_{33} and $\frac{du_3}{d\eta_3}$, rather than these of the individual atoms in a large supercell. In Figure 4(c), we show average Z_{33} for each type of atom (*k*) in the supercell, which is defined as $Z_{33}(k) = \frac{1}{Nn_k} \sum_N \sum_{n_k} Z_{33}(n_k)$, where *N* represents the number of supercells considered for each concentration (we use 2 supercells for each doping/co-doping concentration, hence *N*=2), n_k runs over all the *k*-type atoms in a supercell (e.g., n_{Al}, n_N, n_{Li} and $n_{V/Nb/Ta}$ are 10, 16, 3 and 3 for 37.5% Li and V/Nb/Ta co-doping, respectively). Similarly, we also take average of $\frac{du_3}{d\eta_3}$, which is defined as $\frac{du_3(k)}{d\eta_3} = \frac{1}{Nn_k} \sum_N \sum_{n_k} \frac{du_3(n_k)}{d\eta_3}$. We find that the large increase in the e_{33}^{int} for co-doping is due to the large Z_{33} of the V/Nb/Ta and the enhancement of $\frac{du_3}{d\eta_3}$ compared to these of *w*-AlN (see Figure S.1 and Figure S.2 in the supplementary materials). Now, from Figure 4(c-d), we notice that the Z_{33} remains almost unchanged for Li and V co-doping as a function of concentration, although the $\frac{du_3}{d\eta_3}$ of both Li and V drops significantly at 37.5%, which consequently results a dramatic drop in the e_{33}^{int}, hence also in the total e_{33}.

Piezoelectric materials used in various applications e.g., transducers, energy harvesting, pressure sensors, gyroscopes, and accelerometer operate in the longitudinal vibration mode. Generally a high value of the electromechanical coupling coefficient K_{33}^2 is required for transducers with broader band-width, better axial resolution, and better sensitivity. K_{33}^2, shown in Figure 5(a), is defined as $K_{33}^2 = \frac{e_{33}^2}{\varepsilon_{33} C_{33} + e_{33}^2} \times 100\%$, where ε_{33} is a component of the dielectric tensor (shown in Figure 5(b))[49]. We find that Sc and all co-dopants significantly enhance K_{33}^2 (Figure 5(a)). Our calculated K_{33}^2 values for Sc doping is consistent with the values reported experimentally[50, 51]. For example, the experimentally estimated electromechanical coupling coefficients for Sc doping of 20% and 30% are 10% and 15%, respectively[51]. 37.5% co-doping of Li and Ta in a 1:1 ratio shows the highest K_{33}^2 (20.89%), which is 3.24 times larger than that of pure *w*-AlN. The low K_{33}^2 for Li and V co-doping at 37.5% is due to its decrease in e_{33} (shown in Figure 3(d)). Note that K_{33}^2 of all the co-dopants at 37.5% are lower than that of Sc doped *w*-AlN mainly because ε_{33} for Sc doping does not increase much as the Sc concentration increases (shown in Figure 5(b)). Similar values and trend of increase in ε_{33}[51] or effective ε_{33}, measured for the thin films clamped to the substrate, has also been observed for Sc doping experimentally[34]. Our calculated ε_{33} for *w*-AlN is also close to typical experimental values (~10) in the literature[34, 51]. In general, the K_{33}^2 for

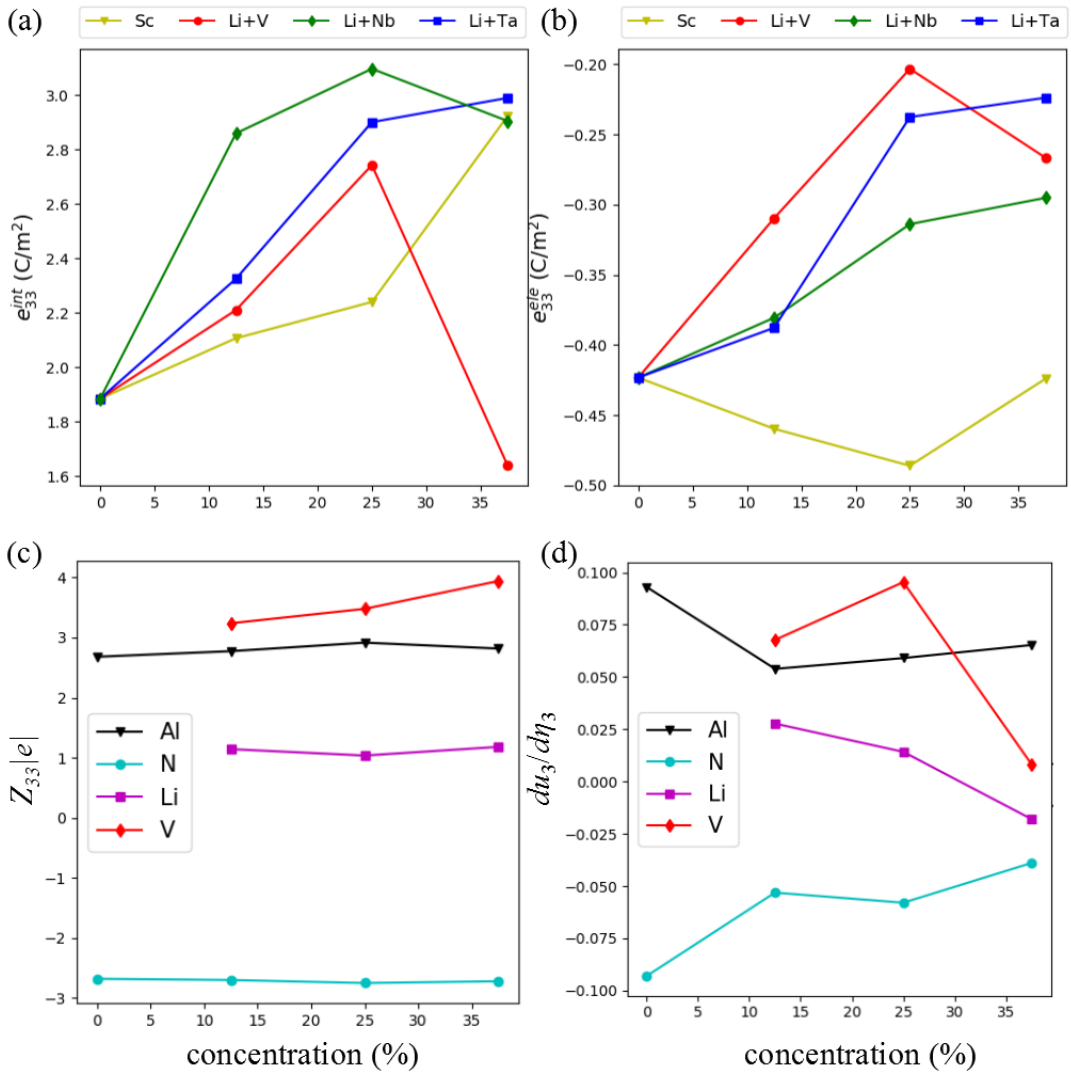

FIGURE 4 (a) The internal coordinate (e_{33}^{int}) and (b) the electronic (e_{33}^{ele}) parts of the e_{33} as a function of doping concentration. The simultaneous significant increase in e_{33}^{int} but decrease in the magnitude of e_{33}^{ele} result enhancement in e_{33} for co-doping. The e_{33}^{int} is proportional to (c) the 33 component of Born effective charge (Z_{33}) tensor and (d) the ($\frac{du_3}{d\eta_3}$), which is the sensitivity of the atomic positions (u_3) in response to a strain along c-direction (η_3). Although the Z_{33} remains almost unchanged for Li and V co-doping as a function of concentration, the $\frac{du_3}{d\eta_3}$ of both Li and V drops significantly at 37.5%, which consequently results a dramatic drop in total e_{33}.

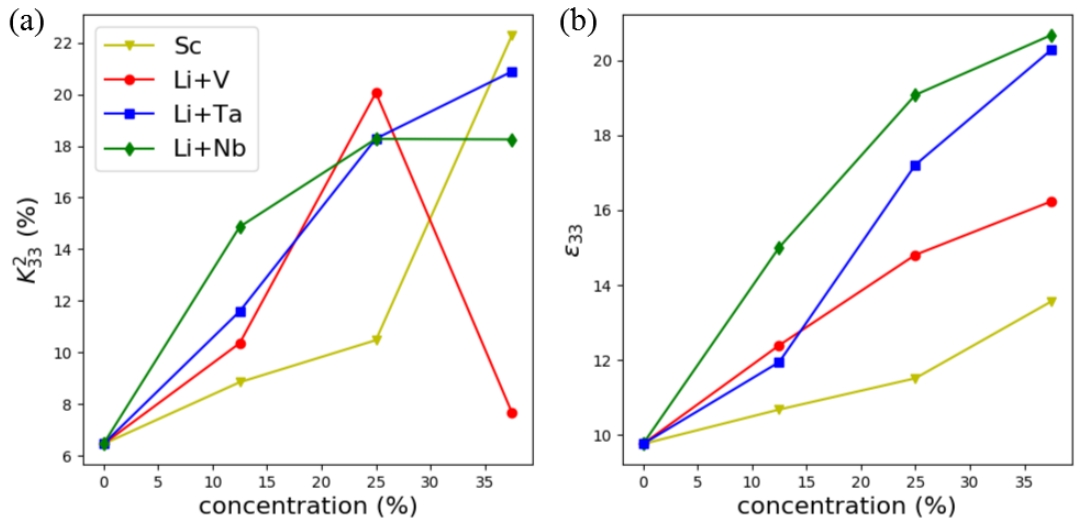

FIGURE 5 (a) The longitudinal electromechanical coupling constant (K_{33}^2) and (b) the zz component of the macroscopic dielectric tensor ϵ_{33} as a function of co-doping and Sc doping concentration in w-AlN.

a device depends collectively on the materials properties of the piezoelectric, the electrodes, and the device design. Here, it should also be mentioned that a high value of $K_{33}^2.Q$ is desired for a resonator with high performance and wide bandwidth, where Q is the mechanical quality factor. The Q determines the loss of an inserted mechanical energy. Generally, the Q is proportional to the stiffness constants[52], although several damping mechanisms e.g, damping at the interface between the piezoelectric and the electrodes, the phonon-phonon dissipation, damping due the quality of the piezoelectric (e.g., scattering of the acoustic wave by the defects), and mechanical energy leakage due to the device fabrication have significant impact[53, 54]. As the C_{33} decreases with the doping concentration, hence we expect a decrease in the Q. Indeed, this has been observed experimentally for Sc[6] and other co-dopants[55].

For many piezoelectric-based actuators, energy harvesters, and sensors, transverse piezoelectric coefficient d_{31} is also an important parameter, and a large d_{31} is desired. We find that co-doping significantly enhances the d_{31} compared to that of pure w-AlN (Shown in Figure 6(a)). Note that d_{31} and d_{32} are equal in pure w-AlN due to its crystal symmetry (space group $P6_3mc$). However, doping locally breaks the symmetry, hence d_{31} and d_{32} are not exactly equal, although they are close in value (See "Supplementary Information"). We can therefore take as a reasonable approximation the average of d_{31} and d_{32} for estimating d_{31}. Note that we also consider two configurations for each co-doping or Sc doping concentration – discussed in the computational details section. Therefore, the reported d_{31} is also the average d_{31} of two configurations at each concentration. 37.5% co-doping of Li and Ta shows the highest d_{31} (-8.45 pC/N), which is about 3.89 times larger than that of pure w-AlN, whereas d_{31} for 37.5% Sc doping is -10.67 pC/N. Larger d_{31} usually guarantees higher figure of merit (FOM), which is an another important parameter for choosing piezoelectric materials for power generation in vibration-based energy harvesters. FOM is defined as $\mathrm{FOM} = \frac{d_{31}^2 Y^2}{\epsilon_{33}}$, where Y is the Hill's Young's modulus (see Figure 2(b))[17]. We find that the co-dopants significantly enhance the FOM compared to that of w-AlN. This is especially obvious for Li and Ta co-doping (see Fig.6(b)). For 37.5% Li and Ta co-doping the FOM is 16.60 GPa, which is 3.27 times higher than that of w-AlN. This is promising for energy harvesters. Due to the low d_{31} the FOM for 37.5% Li and V co-doping, 5.91 GPa, is lower than that for 25% co-doping (10.23 GPa). But this is still twice that of w-AlN. Note that because of low ϵ_{33} of Sc doped w-AlN (see Figure 5(b)), the FOM of Sc doped w-AlN remains higher

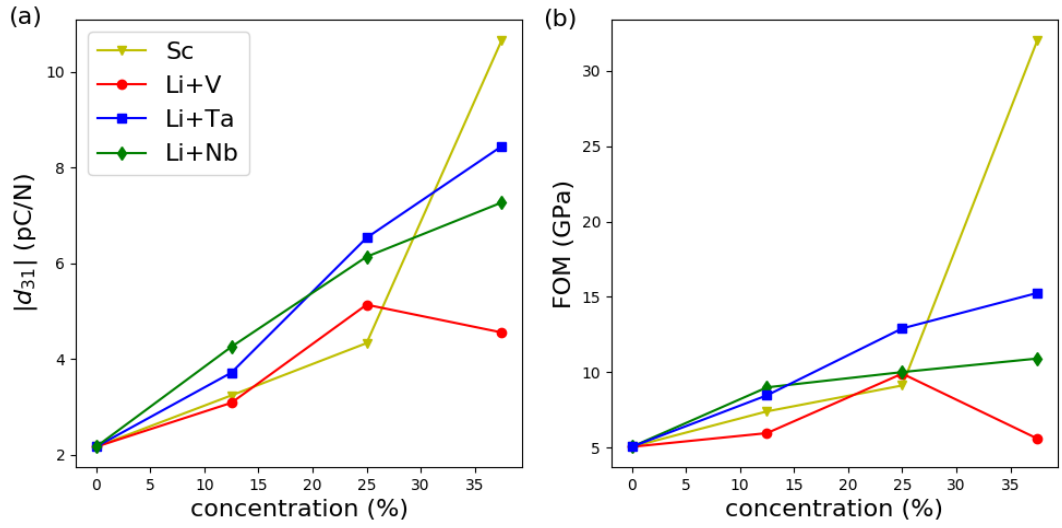

FIGURE 6 (a) the magnitude of the transverse piezoelectric strain constant (d_{31}) and (b) the figure of merit (FOM) for piezoelectric power generation as a function of Sc and co-doping concentration in w-AlN.

than that of the co-dopants for the considered concentration range.

For designing electroacoustic devices e.g. film-bulk acoustic resonators (FBARs) or surface acoustic wave (SAW) resonators for their applications in the frequency filters and duplexers for next generation wireless communication systems, the acoustic wave velocity is an important parameter, which is also sometimes used to estimate the elastic constants in experiments. Compared to other piezoelectrics[53, 56], a high acoustic wave velocity of *w*-AlN is one of the key advantages for high frequency SAW resonators. We compute the elastic wave velocity by solving Christoffel equation $(C_{ijkl}\eta_j\eta_k - \rho v^2\delta_{ij})u_l = 0$, where C_{ijkl} is the elastic co-efficient factor, η represents the propagation direction of the wave, ρ is the mass density, v is the velocity and u stands for the wave polarization[57]. For a given direction, there are three solutions (three velocities): a longitudinal velocity, also known as primary velocity (v_{P}), when the wave polarization is parallel to the wave propagation direction and two transverse velocities, known as secondary velocities (v_{S}), when the wave polarization is perpendicular to the wave propagation direction[57]. Figure 7 shows the calculated elastic wave velocities along the [001] direction, which is usually the important direction for designing devices e.g., resonators or sensors. Our calculated v_{P} and v_{S} for *w*-AlN are 10.58 Km/s^2 and 6.10 Km/s^2, respectively, which are in good agreement with the values in the literature[58, 50]. We find that co-doping and Sc doping decrease both the primary and the secondary wave velocities as the doping concentration increases –again due to the decrease in C_{33} with the doping concentration. This trend is also observed experimentally for Sc doping[50] and Mg and Hf/Zr co-doping[21]. Li and Ta co-doping shows the lowest velocities, which mainly due to the fact that Ta is the heaviest among our considered elements. The velocities at any particular concentration of our considered co-dopants are quite comparable with these of Sc doped *w*-AlN, and also comparable with the velocities in the range of 5-7 km/s for $LiNbO_3$ or $LiTaO_3$ crystals depending on the cuts[53, 56].

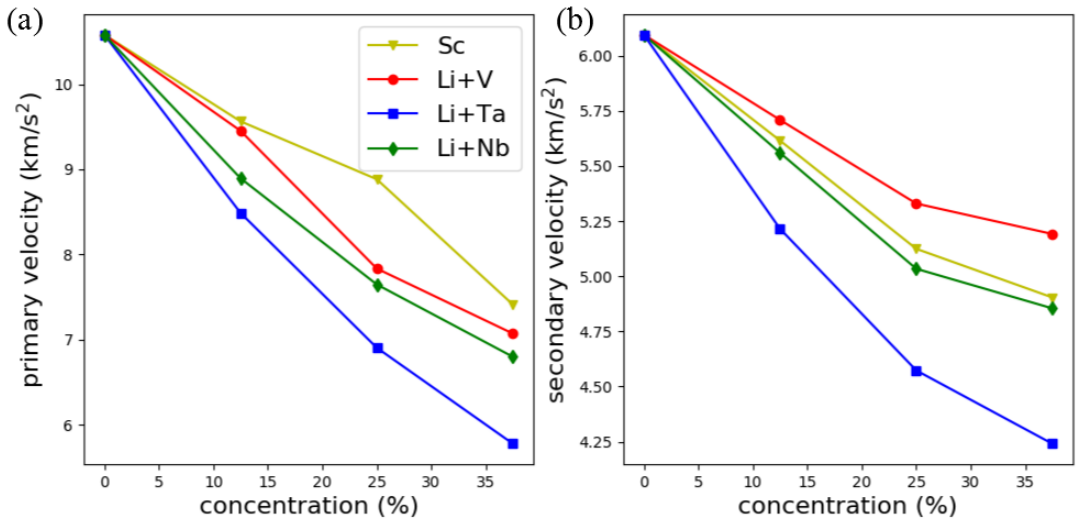

FIGURE 7 (a) The primary (longitudinal) and (b) the average secondary (transverse) acoustic velocity as a function of Sc and co-doping concentration in w-AlN.

4 | CONCLUSION

We show that Li and X (X=V, Nb and Ta) co-doping in 1Li:1X ratio significantly enhances the piezoelectric constants (d_{33} and d_{31}), electromechanical coupling constant (K_{33}^2), and figure of merit for power generation of *w*-AlN, which make these co-doped *w*-AlN are potential lead-free piezoelectric materials for energy harvesting, sensors, and resonators for high frequency RF signals. These parameters are also quite comparable with these of Sc doped *w*-AlN. In fact, these co-dopants outperform Sc doping in terms of piezo-response – especially at 25% concentration – promising that the co-dopants can be good alternative of expensive Sc. Interestingly, the co-doped *w*-AlN also show the possibility of ferroelectric polarization switching with a quite large spontaneous electric polarization about 0.80 C/m^2 with large coercive field of few MV/cm but relatively low dielectric constant of about 20, opening new possibilities in wurtzite nitrides for nanoscale memory applications. Increase in piezoelectric stress constant (e_{33}) with decrease in elastic constant (C_{33}) results enhancement in piezoelectric strain constant (d_{33}). However, the enhancement in K_{33}^2 is not as pronounced as that in d_{33}, because co-doping increases dielectric constant. The longitudinal acoustic wave velocity drops with co-doping or Sc concentration, although the velocity is still comparable with that of commercially used piezoelectric $LiNbO_3$ or $LiTaO_3$ in special cuts.

Acknowledgment

This publication has emanated from research conducted with the financial support of Science Foundation Ireland (SFI) and is co-funded under the European Regional Development Fund under Grant Number 13/RC/2077. MN acknowledges support from SFI through grant number 17/NSFC/5279. The calculations were performed using the high-performance computing facilities of the Tyndall National Institute. We also acknowledge access to computing resources at Irish Centre for High-End Computing (ICHEC).

REFERENCES

[1] H. P. Loebl, M. Klee, C. Metzmacher, W. Brand, R. Milsom, P. Lok, *Materials Chemistry and Physics* **2003**, *79* (2), 143 – 146.

[2] P. Muralt, J. Antifakos, M. Cantoni, R. Lanz, F. Martin, *IEEE Ultrasonics Symposium* **2005**, *1*, 315–320.

[3] R. B. Karabalin, M. H. Matheny, X. L. Feng, E. Defaÿ, G. L. Rhun, C. Marcoux, S. Hentz, P. Andreucci, M. L. Roukes, *Appl. Phys. Lett.* **2009**, *95* (10), 103111.

[4] C. Xiong, X. Sun, K. Y. Fong, H. X. Tang, *Appl. Phys. Lett.* **2012**, *100* (17), 171111.

[5] M. Rinaldi, C. Zuniga, C. Zuo, G. Piazza, *IEEE Transactions on Ultrasonics, Ferroelectrics, and Frequency Control* **2010**, *57* (1), 38–45.

[6] M. Park, Z. Hao, D. G. Kim, A. Clark, R. Dargis, A. Ansari, in *20th International Conference on Solid-State Sensors, Actuators and Microsystems Eurosensors XXXIII (Transducers Eurosensors XXXIII)*, **2019**, pp. 450–453.

[7] G. Piazza, V. Felmetsger, P. Muralt, R. H. Olsson III, R. Ruby, *MRS Bulletin* **2012**, *37* (11), 1051–1061.

[8] N. Sinha, G. E. Wabiszewski, R. Mahameed, V. V. Felmetsger, S. M. Tanner, R. W. Carpick, G. Piazza, *Appl. Phys. Lett.* **2009**, *95* (5), 053106.

[9] H. Campanella, Y. Qian, C. O. Romero, J. Giner, R. Kumar, *2020 IEEE 33rd International Conference on Micro Electro Mechanical Systems (MEMS)* **2020**, 218–221.

[10] M. Akiyama, T. Kamohara, K. Kano, A. Teshigahara, Y. Takeuchi, N. Kawahara, *Adv. Mater.* **2009**, *21* (5), 593–596.

[11] K. R. Talley, S. L. Millican, J. Mangum, S. Siol, C. B. Musgrave, B. Gorman, A. M. Holder, A. Zakutayev, G. L. Brennecka, *Phys. Rev. Materials* **2018**, *2*, 063802.

[12] C. Tholander, I. A. Abrikosov, L. Hultman, F. Tasnádi, *Phys. Rev. B* **2013**, *87*, 094107.

[13] S. Zhang, D. Holec, W. Y. Fu, C. J. Humphreys, M. A. Moram, *J. Appl. Phys.* **2013**, *114* (13), 133510.

[14] S. Fichtner, N. Wolff, F. Lofink, L. Kienle, B. Wagner, *J. Appl. Phys.* **2019**, *125* (11), 114103.

[15] Y. Iwazaki, T. Yokoyama, T. Nishihara, M. Ueda, *Appl. Phys. Express* **2015**, *8* (6), 061501.

[16] C. Tholander, F. Tasnádi, I. A. Abrikosov, L. Hultman, J. Birch, B. Alling, *Phys. Rev. B* **2015**, *92*, 174119.

[17] H. H. Nguyen, H. Oguchi, L. V. Minh, H. Kuwano, *ACS Comb. Sci.* **2017**, *19* (6), 365–369.

[18] B. Wang, K. Aryana, J. T. Gaskins, P. E. Hopkins, S. V. Khare, D. Gall, *Adv. Funct. Mater.* **2020**, *30* (30), 2001915.

[19] S. A. Anggraini, M. Uehara, K. Hirata, H. Yamada, M. Akiyama, *Ceram. Int.* **2020**, *46* (3), 4015 – 4019.

[20] L. V. Minh, M. Hara, T. Yokoyama, T. Nishihara, M. Ueda, H. Kuwano, *IEEE Transactions on Ultrasonics, Ferroelectrics, and Frequency Control* **2015**, *62* (11), 2005–2008.

[21] A. Nagakubo, M. Arita, T. Yokoyama, S. Matsuda, M. Ueda, H. Ogi, M. Hirao, *Jpn. J. Appl. Phys.* **2015**, *54* (7S1), 07HD01.

[22] K. Hirata, H. Yamada, M. Uehara, S. A. Anggraini, M. Akiyama, *ACS Omega* **2019**, *4* (12), 15081–15086.

[23] M. Uehara, H. Shigemoto, Y. Fujio, T. Nagase, Y. Aida, K. Umeda, M. Akiyama, *Appl. Phys. Lett.* **2017**, *111* (11), 112901.

[24] A. M. Holder, S. Siol, P. F. Ndione, H. Peng, A. M. Deml, B. E. Matthews, L. T. Schelhas, M. F. Toney, R. G. Gordon, W. Tumas, J. D. Perkins, D. S. Ginley, B. P. Gorman, J. Tate, A. Zakutayev, S. Lany, *Sci. Adv.* **2017**, *3* (6).

[25] J. P. Perdew, K. Burke, M. Ernzerhof, *Phys. Rev. Lett.* **1996**, *77* (18), 3865.

[26] G. Kresse, J. Furthmüller, *Phys. Rev. B* **1996**, *54* (16), 11169.

[27] G. Kresse, D. Joubert, *Phys. Rev. B* **1999**, *59* (3), 1758.

[28] M. Calandra, *Phys. Rev. Lett.* **2018**, *121*, 026401.

[29] E. Martino, A. Pisoni, L. Ćirić, A. Arakcheeva, H. Berger, A. Akrap, C. Putzke, P. J. W. Moll, I. Batistić, E. Tutiš, L. Forró, K. Semeniuk, *npj 2D Mater. and Appl.* **2020**, *4* (1), 7.

[30] Y. Wang, D. Puggioni, J. M. Rondinelli, *Phys. Rev. B* **2019**, *100*, 115149.

[31] A. van de Walle, P. Tiwary, M. de Jong, D.L. Olmsted, M. Asta, A. Dick, D. Shin, Y. Wang, L.-Q. Chen, Z.-K. Liu, *Calphad* **2013**, *42*, 13 – 18.

[32] H. Momida, T. Oguchi, *Appl. Phys. Express* **2018**, *11* (4), 041201.

[33] T. Nann, J. Schneider, *Chem. Phys. Lett.* **2004**, *384* (1), 150 – 152.

[34] N. Kurz, A. Ding, D. F. Urban, Y. Lu, L. Kirste, N. M. Feil, A. Žukauskaitė, O. Ambacher, *J. Appl. Phys.* **2019**, *126* (7), 075106.

[35] F. Tasnádi, B. Alling, C. Höglund, G. Wingqvist, J. Birch, L. Hultman, I. A. Abrikosov, *Phys. Rev. Lett.* **2010**, *104*, 137601.

[36] K. Tagami, J. Koga, Y. Nohara, M. Usami, *Jpn. J. Appl. Phys.* **2017**, *56* (5), 058004.

[37] F. Mouhat, F. Coudert, *Phys. Rev. B* **2014**, *90*, 224104.

[38] R. Gaillac, P. Pullumbi, F. Coudert, *J. Phys. Condens. Matter* **2016**, *28* (27), 275201.

[39] M. Akiyama, K. Umeda, A. Honda, T. Nagase, *Appl. Phys. Lett.* **2013**, *102* (2), 021915.

[40] M. Dubois, P. Muralt, *J. Appl. Phys.* **2001**, *89* (11), 6389–6395.

[41] H. Momida, A. Teshigahara, T. Oguchi, *AIP Adv.* **2016**, *6* (6), 065006.

[42] J. W. Bennett, K. F. Garrity, K. M. Rabe, D. Vanderbilt, *Phys. Rev. Lett.* **2012**, *109*, 167602.

[43] M. Noor-A-Alam, O. Z. Olszewski, M. Nolan, *ACS Appl. Mater. Interfaces* **2019**, *11* (22), 20482–20490.

[44] B. A. Tuttle, D. A. Payne, J. L. Mukherjee, *MRS Bulletin* **1994**, *19* (7), 20–20.

[45] M. Vopsaroiu, J. Blackburn, M. G. Cain, P. M. Weaver, *Phys. Rev. B* **2010**, *82*, 024109.

[46] T. Mikolajick, S. Slesazeck, M. H. Park, U. Schroeder, *MRS Bulletin* **2018**, *43* (5), 340–346.

[47] Z. Fan, J. Chen, J. Wang, *J. Adv. Dielectr.* **2016**, *06* (02), 1630003.

[48] F. Bernardini, V. Fiorentini, D. Vanderbilt, *Phys. Rev. B* **1997**, *56*, R10024–R10027.

[49] S. Manna, G. L. Brennecka, V. Stevanović, C. V. Ciobanu, *J. Appl. Phys.* **2017**, *122* (10), 105101.

[50] T. Yanagitani, M. Suzuki, *Appl. Phys. Lett.* **2014**, *105* (12), 122907.

[51] G. Wingqvist, F. Tasnádi, A. Zukauskaite, J. Birch, H. Arwin, L. Hultman, *Appl. Phys. Lett.* **2010**, *97* (11), 112902.

[52] D. Wu, Y. Chen, S. Manna, K. Talley, A. Zakutayev, G. L. Brennecka, C. V. Ciobanu, P. Constantine, C. E. Packard, *IEEE Transactions on Ultrasonics, Ferroelectrics, and Frequency Control* **2018**, *65* (11), 2167–2175.

[53] S. Gong, G. Piazza, *IEEE Transactions on Microwave Theory and Techniques* **2013**, *61* (1), 403–414.

[54] Y. Liu, Y. Cai, Y. Zhang, A. Tovstopyat, S. Liu, C. Sun, *Micromachines* **2020**, *11* (630).

[55] T. Yokoyama, Y. Iwazaki, Y. Onda, T. Nishihara, Y. Sasajima, M. Ueda, *IEEE Transactions on Ultrasonics, Ferroelectrics, and Frequency Control* **2015**, *62* (6), 1007–1015.

[56] N. F. Naumenko, *Ultrasonics* **2019**, *95*, 1 – 5.

[57] J. W. Jaeken, S. Cottenier, *Comput. Phys. Commun.* **2016**, *207*, 445 – 451.

[58] M. Kazan, E. Moussaed, R. Nader, P. Masri, *Phys. Status Solidi c* **2007**, *4* (1), 204–207.